

~~CONFIDENTIAL~~

NACA 225

Copy

RM E53104

NACA RM E53104

LOAN COPY: RETURN  
AFWL-WL  
KIRTLAND AFB, NM

0069387

TECH LIBRARY KAFB, NM



## RESEARCH MEMORANDUM

PRELIMINARY DRAG AND HEAT-TRANSFER DATA OBTAINED

FROM AIR-LAUNCHED CONE-CYLINDER TEST VEHICLE

OVER MACH NUMBER RANGE FROM 1.5 TO 5.18

By Wesley E. Messing, Leonard Rabb, and John H. Disher

Lewis Flight Propulsion Laboratory  
Cleveland, OhioDOWNGRADED AT 3 YEAR INTERVALS;  
DECLASSIFIED AFTER 12 YEARS.  
DOD DIR 5200.10

This material contains information affecting the National Defense of the United States within the meaning of the espionage laws, Title 18, U.S.C., and the transmission or revelation of which in any manner to an unauthorized person is prohibited by law.

NATIONAL ADVISORY COMMITTEE  
FOR AERONAUTICS

WASHINGTON

November 16, 1953

OWC 9C 53331

225

~~CONFIDENTIAL~~

Declassified by Authority of LARC Security Classification  
Officer (SCG) Letter dated June 16, 1983  
Maurin F. Lomen

FILE

National Aeronautics and  
Space Administration  
Langley Research Center  
Hampton, Virginia  
23665

NASA

JUN 1 6 1983

Reply to AIN of

139A

TO: Distribution

FROM: 180A/Security Classification Officer

SUBJECT: Authority to Declassify NACA/NASA Documents Dated Prior to  
January 1, 1960

*(informal, correspondence)*  
Effective this date, all material classified by this Center prior to  
January 1, 1960, is declassified. This action does not include material  
derivatively classified at the Center upon instructions from other Agencies.

Immediate re-marking is not required; however, until material is re-marked by  
lining through the classification and annotating with the following statement,  
it must continue to be protected as if classified:

"Declassified by authority of LARC Security Classification Officer (SCO)  
letter dated June 16, 1983," and the signature of person performing the  
re-marking.

If re-marking a large amount of material is desirable, but unduly burdensome,  
custodians may follow the instructions contained in NRB 1640.4, subpart F,  
section 1203.604, paragraph (h).

This declassification action complements earlier actions by the National  
Archives and Records Service (NARS) and by the NASA Security Classification  
Officer (SCO). In Declassification Review Program 807008, NARS declassified  
the Center's "Research Authorization" files, which contain reports, Research  
Authorizations, correspondence, photographs, and other documentation.  
Earlier, in a 1971 letter, the NASA SCO declassified all NACA/NASA formal  
series documents with the exception of the following reports, which must  
remain classified:

Document No.

First Author

E-51A30  
E-53G20  
E-53G21  
E-53K18  
SL-54J21a  
E-55C16  
E-56H23a

Nagey  
Francisco  
Johnson  
Spooner  
Westphal  
Fox  
Himmel

JUN 2 3 1983

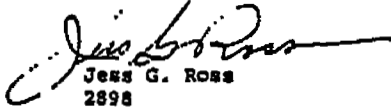
P.02

LARC TECH LIBRARY

804 884 2375

05-05-1987 11:29

If you have any questions concerning this matter, please call Mr. William L. Simkins at extension 3281.

  
 Jess G. Ross  
 2898

Distribution:  
 SDL 031

cc:  
 NASA Scientific and Technical  
 Information Facility  
 P.O. Box 8757  
 BWI Airport, MD 21240

NASA--NIS-5/Security  
 180A/RIAD  
 139A/TU&AO

139A/WLSimkins:elf 06/15/83 (3281)

139A/JS 6-15-83

31-01 HEADS OF ORGANIZATIONS  
 HESS, JANE S.  
 MAIL STOP 184  
 BLOC 1194



0069387

NACA RM E53104

~~CONFIDENTIAL~~

NATIONAL ADVISORY COMMITTEE FOR AERONAUTICS

RESEARCH MEMORANDUM

PRELIMINARY DRAG AND HEAT-TRANSFER DATA OBTAINED FROM AIR-LAUNCHED

CONE-CYLINDER TEST VEHICLE OVER MACH NUMBER RANGE

FROM 1.5 TO 5.18

By Wesley E. Messing, Leonard Rabb, and John H. Disher

SUMMARY

An air-launched cone-cylinder test vehicle designed to obtain data at Mach numbers above 4.0 was rocket boosted by a single internal rocket from a release Mach number of 0.55 to a maximum Mach number of 5.18. The vehicle was launched at an altitude of 35,000 feet, rocket boosted to a velocity of 5150 feet per second at 28,500 feet altitude, and decelerated to a Mach number of 3.50 at 19,000 feet at which point the telemetering transmission terminated,

The total-drag coefficient based on maximum cross-sectional area decreased gradually from 0.31 at a Mach number of 1.75 to 0.145 at a Mach number of 5.18, while the Reynolds number (based on body length) increased from  $31 \times 10^6$  to  $107 \times 10^6$ . At a Mach number of 5.18, the pressure drag on the forebody constituted approximately one-half of the total drag, while one-third was friction drag and one-sixth was base drag. The average skin-friction coefficient based on wetted area as determined from a total-pressure survey rake located 69.63 inches from the cone apex varied from 0.0025 at a Mach number of 1.75 and Reynolds number of  $22.2 \times 10^6$  (based on length to rake) to 0.0010 at a Mach number of 5.15 and Reynolds number of  $92.3 \times 10^6$ . The experimental friction-drag coefficients, in general, were slightly lower than Van Driest's theoretical values for similar wall-temperature conditions. The ratio of base pressure to ambient pressure reached a minimum value of 0.17 at a Mach number of 5.0 during deceleration after rocket burnout.

The convective heat-transfer coefficients as obtained from a single temperature measurement were approximately 15 to 20 percent lower than those predicted by the recent theory of Van Driest for similar wall-temperature conditions. A maximum skin temperature of  $1240^\circ \text{R}$  was recorded during the flight.

~~CONFIDENTIAL~~

SWC 9C 53331

3013

1-CD

## INTRODUCTION

At the present time, there is a need for a reliable, short-range, research test vehicle that would be capable of obtaining data at Mach numbers above 4.0 under actual free-flight atmospheric conditions. The test vehicle should be simple in design, easily fabricated, and relatively inexpensive to make it expendable.

In a preliminary investigation, one such vehicle was designed at the NACA Lewis laboratory; the free-flight drop technique was used in testing the vehicle at the NACA Langley Pilotless Aircraft Research Station, Wallops Island, Virginia. A 20° (total angle) cone-cylinder vehicle housing a solid-propellant production-type rocket engine having a nominal rated impulse of 18,000 pound-seconds was launched from an F-82 airplane at a pressure-altitude of 35,000 feet. The rocket engine fired after the vehicle left the airplane and accelerated it to supersonic velocities. At the end of the rocket-boost period, the test vehicle decelerated because of its drag. Data were obtained from a 10-channel telemetering unit installed in the nose of the test vehicle and were recorded at ground receiving stations.

The data obtained from this preliminary test vehicle consisted of acceleration, velocity, ambient pressure, net thrust (during rocket-boost period), total drag, pressure drag, friction drag, base drag, and convective heat-transfer coefficient. The Mach number range encountered was 0.55 to 5.18 with a variation in Reynolds number (based on body length) of  $9 \times 10^6$  to  $107 \times 10^6$ .

## APPARATUS AND PROCEDURE

The test vehicle consisted basically of a 20° cone with a cylindrical afterbody stabilized by a cruciform fin arrangement. The vehicle had a maximum diameter of 9.25 inches and a fineness ratio of 8.6. The engine used for this investigation was a solid-propellant rocket, Jato 6-KS-3000, T-40. A photograph of the test vehicle is given in figure 1. This photograph illustrates the relative size of the rocket engine to the test vehicle. The schematic sketch presented in figure 2 includes the general dimensions and specifications of the test vehicle. The vehicle was fabricated in three sections (fig. 3). The forward section, which was electrically insulated from the center section, served as the telemeter antenna. In order to make the vehicle aerodynamically stable at the high Mach numbers, it was necessary to add a 13.5-pound lead ballast in the forward section. The metal skin was seam-welded 22-gauge (0.031 in.) stainless steel, type 430, riveted to threaded ring sections and was hand polished to a smooth outer surface. The fins were fabricated out of 11-gauge (0.125 in.) carbon steel and had a total span of 25.25 inches with a root chord of 11.5 inches. The general specifications

and the rated performance of the rocket engine are given in table I as obtained from reference 1. In order to insure satisfactory rocket operation at the low temperatures existing at high altitude, the rocket engine was enclosed in an electric heater blanket which maintained a rocket temperature of approximately 100° F, prior to rocket firing.

The data were radio-telemetered to the ground receiving stations from a 10-channel telemeter unit located in the nose of the vehicle. The stations at which the measurements were taken are included in figure 2. The temperature sensing element consisted of a small resistance wire pickup which had a low heat capacity and an extremely fast response. This pickup is fully described in reference 2. A sketch showing the installation of the element is given in figure 4. A radar-tracking unit, type SCR-584, with optical tracking facilities was used to determine the space position of the test vehicle. An atmospheric survey was conducted by the launching airplane immediately after the drop in order to determine the ambient pressure and temperature encountered by the test vehicle throughout the flight altitude range. A weather balloon was released from the ground and tracked by radar in order to obtain wind corrections for the computed space velocity. The performance was computed according to the method given in the appendix.

## RESULTS AND DISCUSSION

Continuous data were obtained from the test vehicle for 16.4 seconds of the flight at which time the telemetering carrier signal terminated. It is believed that the telemetering unit in the vehicle failed because of the excessive heat due to the high skin temperatures in the telemeter section of the missile. This difficulty could be overcome in future test vehicles by adequate thermal insulation. The optical tracking facilities of the radar unit failed to maintain contact with the test vehicle after 7.8 seconds and no ground-tracking data were obtained thereafter.

### Primary Data

Free-stream conditions. - Figure 5 gives the time history, after release, of the variation in velocity and pressure-altitude. At 4.8 seconds after release, the rocket ignited and accelerated the test vehicle from a velocity of 550 feet per second to 5150 feet per second at 11.2 seconds at which time the test vehicle had reached a pressure-altitude of approximately 28,500 feet. After the termination of rocket thrust, the vehicle decelerated to a velocity of 3450 feet per second at a pressure-altitude of 19,000 feet, at which point the telemeter carrier signal terminated.

The Mach number and Reynolds number (based on body length and free-stream conditions) are shown on figure 6. In a time period of

6.4 seconds, the test vehicle accelerated from a Mach number of 0.55 to a maximum value of 5.18 with an increase in Reynolds number of from  $9 \times 10^6$  to  $1.07 \times 10^6$ .

The horizontal range covered during this flight is shown in figure 7. In order to permit an extrapolation of the actual trajectory to the impact point, comparison is made with the predicted trajectory as computed from estimated thrust and drag values. There is fair agreement between the two; this would indicate that a horizontal range of approximately 15.9 miles was encountered during this investigation.

Total-pressure measurements. - A time history of the total pressure as measured (no shock corrections applied) during the flight is shown in figure 8. The five measurements were taken 7.53 calibers (69.63 in.) from the apex of the vehicle. Four tubes were spaced within 0.81 inch of the skin (dimensions given in fig. 8) to obtain a total-pressure profile through the boundary layer. The fifth tube was placed well outside any predictable boundary layer in order to obtain the total pressure that could be used to compute the flight speed.

A maximum total pressure of 19,800 pounds per square foot absolute was recorded from this tube at 11.2 seconds. Correcting for the total-pressure shock losses (normal and oblique from the cone) at a Mach number of 5.18 indicates a free-stream total pressure of 400,000 pounds per square foot. The total-pressure measurements taken 0.81 inch from the skin were in close agreement with those taken at 2.50 inches, indicating that the boundary layer at station 69.63 was less than 0.81-inch thick during the flight.

The telemetering channel transmitting the total pressure as measured 0.56 inch from the shell failed at 9.4 seconds, and the measurement at 0.81 inch from the shell terminated at 15 seconds. The other three (2.50, 0.31, and 0.06 in. from the shell) transmitted until the carrier wave terminated at 16.4 seconds. The measurements 0.31 and 0.06 inch from the shell appear questionable during the latter part of flight. Laboratory tests on the instrumentation indicated that the lag in total-pressure measurement was insignificant for the rates of change of pressure encountered during this flight.

Static-pressure measurements. - Static-pressure measurements were taken on the cone, the shell, and the base of the test vehicle. Time histories of these data are shown in figure 9. The cone pressure which was measured at station 17 (1.84 calibers from the cone) increased sharply at 4.9 seconds and continued to rise under the combined influence of increasing Mach number and decreasing altitude from a minimum of 540 pounds per square foot absolute to a maximum of approximately 1880 pounds per square foot absolute. The change in slope of the cone-pressure

3013

curve, as well as of the shell- and base-pressure curves, at approximately 5.3 seconds is associated with the model passing through a Mach number of 1.0 at this time. Because of a lack of radar data during the trajectory, it was necessary to calculate the free-stream static pressure from the shell-static-pressure measurement. This shell-static-pressure measurement (7.53 calibers from apex and  $90^\circ$  from the survey rake) was influenced by the flow expansion about the cone-cylinder junction and was corrected in accordance with reference 3.

The base-pressure measurement showed a suction effect throughout the supersonic part of the flight except for a short time after rocket ignition (4.8 sec) when it was affected by a momentary pressure surge at rocket ignition. The discontinuity in the data at 12.4 seconds is thought to be associated with rocket burnout.

Net acceleration. - Longitudinal accelerometer measurements were taken during the flight and the time history of the net acceleration (excluding gravity) is shown in figure 10. After the rocket ignited, a peak net acceleration of 32.5 g's was momentarily recorded; this decreased to 22.5 g's within approximately 1 second. At about 7.0 seconds after release, the net acceleration started gradually to increase and reached a value of about 30.5 g's at 9 seconds after release. This increase in acceleration during the latter part of the boost phase was a result of the combination of increasing rocket thrust (characteristic of this particular rocket) and decreasing vehicle weight. At 9.6 seconds, the rocket engine began to burn out and the net acceleration declined rapidly to -11 g's at 12.5 seconds. Thereafter, the net accelerometer was responding only to the drag forces acting on the vehicle. The accelerometer telemeter channel terminated at 15 seconds.

Calculation of total rocket impulse based on the accelerometer measurements and the drag calculations indicates a value of about 23,000 pound-seconds for this flight. This agrees approximately with the high-temperature values specified in table I when a theoretical altitude correction is applied to the sea-level values.

Skin temperatures. - Skin temperature was measured on the inside of the cylindrical shell at a point 3.28 calibers from the apex. The data are shown in figure 11 and compared with the ambient temperature, the free-stream total temperature, and the adiabatic wall temperature for an assumed turbulent-boundary-layer recovery factor of 0.89. Unfortunately, it wasn't possible to compute the temperature recovery from the data; however, in reference 4, a value of 0.89 was obtained experimentally with an NACA RM-10 missile at Mach numbers up to 2.48. This value was in good agreement with the value predicted by theory ( $\beta = Pr^{1/3}$ ) in reference 5 for turbulent boundary layer on a flat plate. The skin temperature varied from  $440^\circ$  R to a maximum value of  $1240^\circ$  R. The data beyond 14.2 seconds



appear questionable and suggest possible malfunctioning of the telemeter channel, since the telemeter signal ceased 2.2 seconds later.

### Drag Results

Pressure drag. - The pressure-drag coefficient based on maximum cross-sectional area of the conical section of the test vehicle is shown in figure 12 as a function of Mach number. The corresponding ratio of cone to free-stream static pressure is also shown and is compared with theoretical values from reference 3. It may be seen that, during acceleration, the agreement between experiment and theory is excellent but that, during deceleration, the experimental values are as much as 10 percent higher than theoretical; again, questionable telemeter accuracy during the latter part of the flight is suggested. During the acceleration phase, the pressure-drag coefficient varied from 0.12 at a Mach number of 1.75 to 0.077 at a Mach number of 5.18.

Base drag. - Figure 13 shows the variation of base static-pressure ratio and drag coefficient (based on maximum cross-sectional area) with flight Mach number. Data are shown for the accelerating phase where the rocket exhaust is issuing from the center of the annular base and for the decelerating phase without the rocket exhaust. It was estimated that the static pressure at the rocket-nozzle exit varied between approximately 15 and 18 pounds per square inch absolute during acceleration to a Mach number of 4.4. Beyond this point, the rocket exhaust pressure gradually declines as the rocket thrust terminates.

Except momentarily when the rocket first ignited, the pressure on the base was less than ambient throughout the flight. The underexpanded rocket exhaust influences the base pressure, and the inflections in the base-pressure-ratio curve during rocket operation are believed to be a result of the variations in the estimated rocket-nozzle-exit static pressure. At a Mach number of 5.0 in the decelerating phase, the base pressure was only 17 percent of the ambient pressure.

The base-drag coefficient varied from a maximum value of 0.093 at a Mach number of 1.55 to 0.028 at a Mach number of 5.18. The base drag was computed on the basis of an annular area of 0.331 square feet during rocket operation and on the basis of the complete cross-sectional area, 0.467 square feet (see fig. 2), during deceleration.

Friction drag. - The friction drag acting on the external surface of the test vehicle was determined by the usual method of obtaining the momentum decrement in the boundary layer resulting from the viscous shear forces. A survey of the boundary layer was conducted by means of a total-pressure rake and a flush static orifice located 7.53 calibers (69.63 in.)

from the apex of the vehicle. Assuming that the measured static pressure remained constant through the boundary layer, it was possible to compute the Mach number distribution or profile shown in figure 14 for the various free-stream Mach numbers and Reynolds numbers encountered.

The velocity distribution through the boundary layer was computed from this Mach number distribution by determining the temperature distribution through the boundary layer in accordance with the theoretical relation derived by Crocco in reference 6 and modified in reference 7.

In solving for the boundary-layer temperature distribution, it was assumed that the skin temperature at the total-pressure rake station was the same as at the point of temperature measurement. In order to define the boundary-layer thickness  $\delta$ , it was further assumed that a logarithmic relation exists between the ratio of local velocity in the boundary layer to the velocity outside of the boundary layer and the distance from the point of measurement to the shell,  $V/V_\delta = (y/l)^n$ . When the velocity ratio is plotted against distance from the shell on logarithmic coordinates, the intercept on the distance scale of a straight line extrapolation to a velocity ratio of unity defines the boundary-layer thickness.

Comparison of the boundary-layer data with the power law has been made by plotting the distance ratio  $y/\delta$  against the velocity ratio  $V/V_\delta$  as shown in figure 15, which indicates that, for the conditions encountered in this investigation, an exponent of  $1/9$  is applicable throughout the Mach number and Reynolds number ranges.

The friction drag expressed in coefficient form based on wetted area is shown in figure 16 as a function of Mach number and Reynolds number. Comparison is made with the Van Driest theory on the mean friction drag resulting from a fully turbulent boundary layer on a flat plate as given in reference 8. Also shown is the incompressible, mean, skin-friction coefficient as obtained from the Kármán-Schoenherr equation,  $0.242/C_{f,i}^{1/2} = \log(\text{Re } C_{f,i})$ . The experimental data and the Van Driest theoretical curves are also shown in the more general form as a ratio to the incompressible case. The data were obtained under conditions of heat transfer from the boundary layer to the wall; the experimental wall-temperature ratio  $t_w/t_\delta$  and the adiabatic wall-temperature ratio  $t_{aw}/t_\delta$  are therefore included. As the Mach number increases, the difference between the two experimental temperature ratios increases; this indicates an increasingly higher rate of heat transfer from the boundary layer to the wall. As the Van Driest theory includes the effect of heat transfer on the friction drag, the theoretical curves were computed for the insulated wall case and for  $t_w/t_\delta = 1.0$  and  $t_w/t_\delta = 2.0$ . The insulated wall condition is one of zero heat transfer and would result if the wall temperature equaled the adiabatic wall temperature, that is,  $t_w/t_{aw} = 1.0$ .

In general, the experimental data were in good agreement with the theoretical curve based on the insulated wall condition and slightly lower than that predicted for the flight conditions encountered,  $1.0 < t_w/t_8 < 2.0$ . However, as the experimental friction drag was influenced by a laminar boundary layer of unknown length existing on the test vehicle, it would be expected that the over-all mean friction drag as measured would not necessarily agree with that predicted for a fully turbulent boundary layer on a flat plate. The experimental friction-drag coefficient decreased in value with increasing Mach number and Reynolds number from 0.0025 at a Mach number of 1.75 to 0.0010 at a Mach number of 5.15.

Figure 17 illustrates the total friction-drag coefficient when based on the maximum cross-sectional area as a function of Mach number and Reynolds number. The total friction drag was obtained by applying the mean friction-drag coefficient based on the wetted area up to the rake station (fig. 16) to the entire wetted area of the test vehicle including the fins. The total friction drag was then expressed in coefficient form based on free-stream conditions and cross-sectional area as shown in figure 17. The total friction-drag coefficient decreased gradually with increasing Mach number and Reynolds number from a value of 0.09 at a Mach number of 1.75 to 0.038 at a Mach number of 5.18. Friction-drag data were not computed for the decelerating portion of the flight because of the questionable accuracy of the total-pressure measurements.

Total drag. - The total-drag coefficient based on maximum cross-sectional area is also shown in figure 17 as a function of Mach number and the corresponding Reynolds number values. The total-drag-coefficient curve for accelerating flight is the summation of the individual drag coefficients based on pressure measurements as previously discussed. The total-drag coefficient decreased gradually from 0.31 at a Mach number of 1.75 to 0.145 at a Mach number of 5.18; this decrease was accompanied by an increase in Reynolds number from  $31 \times 10^6$  to  $107 \times 10^6$ . At a Mach number of 5.18, the pressure drag on the forebody accounted for approximately one-half of the total drag; the friction drag on the shell and fins accounted for one-third; and the base drag accounted for only one-sixth. The total drag during deceleration, based on accelerometer measurements, is also shown in figure 17. Higher total drag during deceleration would be expected because of the increase in effective base area and the lower base pressures encountered after rocket burnout.

#### Heat-Transfer Results

Heat-transfer computations were made from the skin-temperature measurements at station 30.25 according to the procedure outlined in the appendix. Errors arise in such computations because of temperature lag

across the skin thickness, radiation losses both to the outside and inside of the test vehicle, heat losses due to conduction from skin to bulkheads, and other small errors inherent in the telemetering system which are described in more detail in reference 2. The effects of these factors on the heat-transfer coefficient have been estimated and were found to be approximately 4 to 8 percent during the accelerating portion of the flight. Heat-transfer calculations were not made after 11 seconds because of increasing errors in calculation and questionable telemeter accuracy.

The local convective heat-transfer coefficient  $h$ , is shown in figure 18 as a function of Mach number and Reynolds number (based on free-stream conditions and length of 30.25 in.). The heat-transfer coefficient increased with increasing values of Mach number and Reynolds number from 0.0098 at a Mach number of 1.75 to 0.0171 at a Mach number of 5.15. Figure 18 also shows the heat-transfer data expressed in dimensionless form as Stanton number  $St$ . Comparison is also made with the theoretical values of Stanton number (Van Driest, ref. 8) for the insulated wall case and for  $t_w/t_g = 1.0$  and  $t_w/t_g = 2.0$ . The experimental values are in good agreement with predicted values for the insulated wall case and are seen to be approximately 15 to 20 percent lower than the values predicted for the wall-temperature ratios, 1.0 and 2.0. The experimental Stanton number decreased with an increase in Mach number and Reynolds number from a value of 0.0095 at a Mach number of 1.75 to 0.0046 at a Mach number of 5.15.

#### SUMMARY OF RESULTS

In order to obtain supersonic data at Mach numbers above 4.0 and at high Reynolds numbers, an air-launched test vehicle was designed and one such model was flown with the following results:

1. The cone-cylinder fin-stabilized vehicle was successfully rocket-boosted by a single, internal, production-type rocket from a launching Mach number of 0.55 to a maximum Mach number of 5.18 at a pressure-altitude of 28,500 feet with a corresponding variation in Reynolds number (based on body length) of  $9 \times 10^6$  to  $107 \times 10^6$ . The horizontal range covered by the flight was estimated to be 15.9 miles.
2. Continuous telemetering data were obtained up to 16.4 seconds after release. The test vehicle during this time period passed through the peak velocity condition (5150 ft/sec) and decelerated to a Mach number of 3.50. The telemetering unit failed at 16.4 seconds, probably because of excessive heat in the telemetering section.
3. The total-drag coefficient decreased gradually from 0.31 at a Mach number of 1.75 to 0.145 at a Mach number of 5.18 with an increase in

Reynolds number from  $31 \times 10^6$  to  $107 \times 10^6$ . At a Mach number of 5.18, the pressure drag on the forebody constituted approximately one-half of the total drag; the friction drag on the shell and fins accounted for one-third; and the base drag accounted for one-sixth.

4. The ratio of base pressure to ambient pressure reached a minimum value of 0.17 at a Mach number of 5.0 during deceleration after rocket burnout.

5. The average skin-friction coefficient based on wetted area as determined from a total-pressure survey rake, located 69.63 inches from the vehicle apex, varied from 0.0025 at a Mach number of 1.75 and a Reynolds number (based on body length to the rake) of  $22.2 \times 10^6$  to 0.0010 at a Mach number of 5.15 and a Reynolds number of  $92.3 \times 10^6$ . The experimental friction coefficients, in general, were slightly lower than Van Driest's theoretical values for similar wall-temperature conditions.

6. The experimental convective heat-transfer coefficients as obtained from a single thermocouple were approximately 15 to 20 percent lower than those predicted by Van Driest's theory for similar wall-temperature conditions. A maximum skin temperature of  $1240^\circ \text{R}$  was recorded during the flight.—

Lewis Flight Propulsion Laboratory  
National Advisory Committee for Aeronautics  
Cleveland, Ohio, September 2, 1953

3013

## APPENDIX - GENERAL METHOD OF CALCULATION

## Symbols

The following symbols are used in this report:

A	maximum cross-sectional area, sq ft, (0.467)
$A_w$	wetted surface area, sq ft, (11.44 to rake, 17.94, total)
a	local speed of sound, ft/sec
$a_n$	net acceleration, g's
$C_D$	drag coefficient, $2D/\gamma P_0 M_0^2 A$
$C_F$	mean skin-friction coefficient, $2D_F/\gamma P_0 M_0^2 A_w$
$C_{F,i}$	incompressible mean skin-friction coefficient
c	specific heat of skin, Btu/(lb)(°R)
$c_p$	specific heat of air at constant pressure, Btu/(slug)(°R)
D	drag force, lb
$D_F$	friction-drag force, lb
G	skin factor, $cxw$ , Btu/(sq ft)(°R)
g	acceleration due to gravity, ft/sec <sup>2</sup>
h	local heat-transfer coefficient, $\frac{G \frac{dt_w}{d\theta}}{(t_{aw} - t_w)}$ , Btu/(sec)(sq ft)(°R)
J	mechanical equivalent of heat, 778 ft-lb/Btu
k	thermal conductivity of air, Btu/(sec)(ft)(°R)
l	length, ft
M	Mach number
n	exponent of power law
P	total pressure, lb/sq ft

Pr	Prandtl number, $c_p \mu / k$
p	static pressure, lb/sq ft
q	quantity of heat, Btu
R	horizontal range, ft
Re	Reynolds number, $\rho_0 V_0 l / \mu$
St	Stanton number, $h / c_p \rho_0 V_0$
T	total temperature, $^{\circ}R$
t	static temperature, $^{\circ}R$
V	velocity, ft/sec
w	specific weight of skin material, lb/cu ft
x	skin thickness, ft
y	radial distance from external surface of shell, ft
$Z_p$	pressure-altitude, ft
$\beta$	recovery factor
$\gamma$	ratio of specific heat of air at constant pressure to specific heat of air at constant volume
$\delta$	boundary-layer thickness, ft
$\theta$	time, sec
$\mu$	coefficient of viscosity of air, lb-sec/sq ft
$\rho$	density of air, slugs/cu ft
$\tau$	viscous shear stress, lb/sq ft

## Subscripts:

A	back of normal shock
aw	adiabatic wall
b	base

c cone pressure  
f friction  
O free stream  
t total  
w wall  
δ just outside of boundary layer

### Calculations

In computing the free-stream conditions encountered by the test vehicle, the free-stream static pressure was obtained from a flush static orifice located on the cylindrical section of the vehicle at station 69.63. Because of the effect of flow expansion about the cone-cylinder junction, the data were corrected in accordance with reference 3 to obtain the free-stream static pressure. From the atmospheric survey conducted by the launching airplane, it was possible to correlate the free-stream static temperature with the static pressure. The velocity was then computed by integrating the total acceleration as obtained from accelerometer measurements and also from the total- and static-pressure measurements obtained at station 69.63. A faired curve through these data points was used to obtain the final free-stream velocity values from which the free-stream Mach number could be obtained. The total temperature was computed in a manner similar to the method suggested in reference 9 in which the variation of the specific heat of air with temperature was considered because of the high stagnation temperatures involved.

The Reynolds number was computed according to the general formula

$$Re = \frac{\rho_0 V_0 l}{\mu}$$

where the coefficient of viscosity  $\mu$  was based on the free-stream static temperature in accordance with Sutherland's formula.

The mean friction drag was determined from the boundary-layer total-pressure survey and a surface static-pressure measurement as obtained at station 69.63. It was assumed that the static pressure as measured remained constant through the boundary layer and that any static-pressure gradient existing axially along the surface would have a negligible effect on the friction drag. It was also assumed that the wall temperature at station 69.63 would be similar to the wall temperature measured at station 30.25.



The Mach number profile through the boundary layer was obtained from the ratio of static to total pressure as determined by use of the conventional equation

$$\frac{P_A}{P} = \frac{\left(\frac{\gamma+1}{2} M^2\right)^{\frac{\gamma}{\gamma-1}}}{\left(\frac{2\gamma}{\gamma+1} M^2 - \frac{\gamma-1}{\gamma+1}\right)^{\frac{1}{\gamma-1}}} \quad (1)$$

The static-temperature profile through the boundary layer was determined by the method of Crocco (ref. 6) wherein a Prandtl number of 1.0 and a steady-state condition were assumed. This method was modified in accordance with reference 7 by including a temperature-recovery factor  $\beta$  equal to 0.89 in order to obtain the adiabatic wall temperature instead of the stagnation temperature when the heat transfer is zero. The equation is as follows:

$$t = t_\delta + (t_w - t_{aw}) \left(1 - \frac{Ma}{V_\delta}\right) + \beta \left[ \frac{V_\delta^2 - (Ma)^2}{2Jc_p} \right] \quad (2)$$

The temperature just outside the boundary layer  $t_\delta$  was obtained by computing the local Mach number just outside the boundary layer and assuming no total-temperature change from the free-stream condition. The temperature  $t_\delta$  could then be computed as

$$t_\delta = \frac{T_0}{\left(1 + \frac{\gamma-1}{2} M_\delta^2\right)} \quad (3)$$

where  $\gamma$  varied from 1.36 to 1.40 depending on the value of  $t_\delta$ . The adiabatic wall temperature  $t_{aw}$  was computed for an assumed temperature-recovery factor of 0.89 as

$$t_{aw} = t_\delta + 0.89 (T_0 - t_\delta) \quad (4)$$

The known Mach number and temperature profiles through the boundary layer as well as the free-stream conditions were used to determine the mean friction drag acting on the external surface by the usual method of obtaining the momentum decrement in the boundary layer. For convenience, the following equation which expresses the friction drag, in coefficient form, in terms of free-stream dynamic pressure and wetted surface area was used in this investigation:

$$C_f = \frac{4\pi r}{r_0 A_w M_0^2} \left( \frac{p_w}{p_0} \right) \left\{ \int_{y=0}^{y=\delta} \left[ MM_\delta \left( \frac{a_\delta}{a} \right) - M^2 \right] y \, dy \right\} \quad (5)$$

where  $y$  is the radial distance outward from the surface of shell.

In order to obtain the total friction drag of the entire vehicle, the mean coefficient as obtained from equation (5) was applied to the total wetted area of the vehicle including the fin area.

Heat-transfer computations were based on a single wall-temperature measurement at station 30.25. Because of the telemetering failure at 16.4 seconds, the computations could only be made during the transient condition when the wall was absorbing heat from the boundary layer. In these computations, the method suggested in reference 2 was used. It was assumed that the heat losses due to radiation and conduction could be considered as negligible. Writing a heat balance between the boundary layer and the wall and determining the time rate of change of heat absorbed by the wall result in

$$\frac{dq}{d\theta} = h A (t_{aw} - t_w) \quad (6)$$

and

$$\frac{dq}{d\theta} = GA \frac{dt_w}{d\theta} \quad (7)$$

therefore

$$h = \frac{G \frac{dt_w}{d\theta}}{t_{aw} - t_w} \quad (8)$$

The wall properties of the metal  $G$  were obtained from reference 10 which presents data for a 13-percent-chromium steel similar to type 430 stainless. The experimental heat-transfer coefficient  $h$  was computed from equation (8).

The convective heat-transfer coefficient can also be presented in the dimensionless form as Stanton number  $St$ , which can be defined on the basis of the properties of air in the free-stream as

$$St = \frac{h}{c_p \rho_0 V_0} \quad (9)$$

## REFERENCES

1. Anon.: Free Flight Rocket Materiel Characteristics. Rep. No. A-10-a, Tech. and Eng. Div., Rocket Div. Branch, Redstone Arsenal, Huntsville (Ala.).
2. Fricke, Clifford L., and Smith, Francis B.: Skin-Temperature Telemeter for Determining Boundary-Layer Heat-Transfer Coefficients. NACA RM L50J17, 1951.
3. Clippinger, R. F., Giese, J. H., and Carter, W. C.: Tables of Supersonic Flows About Cone Cylinders. Pt. I: Surface Data. Rep. No. 729, Ballistic Res. Labs., Aberdeen Proving Ground (Maryland), July 1950. (Proj. TB3-0108H of Res. and Dev. Div., Ord. Dept.)
4. Chauvin, Leo T., and deMoraes, Carlos A.: Correlation of Supersonic Convective Heat-Transfer Coefficients from Measurements of the Skin Temperature of a Parabolic Body of Revolution (NACA RM-10). NACA RM L51A18, 1951.
5. Squire, H. B.: Heat Transfer Calculation for Airfoils. R. & M. No. 1986, British A.R.C., 1942.
6. Crocco, Luigi: Transmission of Heat from a Flat Plate to a Fluid Flowing at a High Velocity. NACA TM 690, 1932.
7. Rumsey, Charles B., and Loposer, J. Dan: Average Skin-Friction Coefficients from Boundary-Layer Measurements in Flight on a Parabolic Body of Revolution (NACA RM-10) at Supersonic Speeds and at Large Reynolds Numbers. NACA RM L51B12, 1951.
8. Van Driest, E. R.: Turbulent Boundary Layer in Compressible Fluids. Jour. Aero. Sci., vol. 18, no. 3, Mar. 1951, pp. 145-161.
9. Evans, Philip J., Jr.: Analytical Investigation of Ram-Jet-Engine Performance in Flight Mach Number Range from 3 to 7. NACA RM E51H02, 1951.
10. National Physical Laboratory, Physics Division: The Physical Properties of a Series of Steels - Part II. Jour. Iron and Steel Inst. (London), vol. CLIV, no. 2, 1946, pp. 83P-84P.

3013

TABLE I. - SPECIFICATIONS AND RATED PERFORMANCE OF JATO-6-KS-3000,  
T-40 ROCKET ENGINE AT SEA LEVEL

[Data from ref. 1.]

Specifications

Outside diameter (chamber), in. . . . .	8.265
Total length, in. . . . .	47.69
Total weight (unburnt), lb . . . . .	132
Total weight (burnt), lb . . . . .	29
Nozzle expansion angle (included), deg . . . . .	30
Throat area, sq in. . . . .	3.38
Nozzle-exit area, sq in. . . . .	19.635

Performance

Temperature of rocket propellant, °F . . . . .	-20	70	130
Maximum thrust, lb . . . . .	3,300	4,500	5,500
Average thrust, lb . . . . .	2,500	3,100	3,500
Total impulse, lb-sec . . . . .	18,000	20,000	21,000
Specific impulse, lb-sec/lb . . . . .	175	195	204
Burning time, sec . . . . .	6.8	6.0	5.2

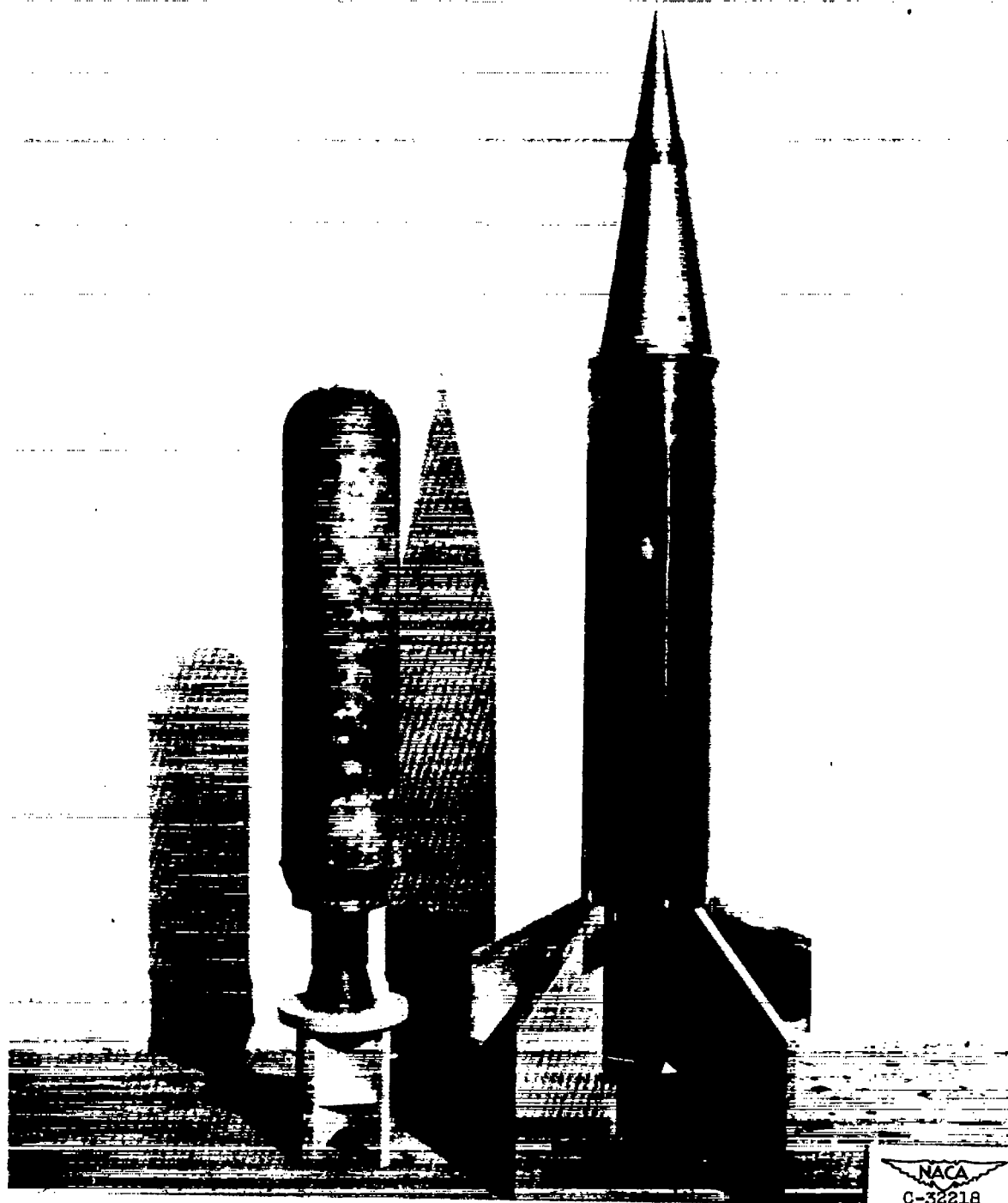


Figure 1. - Air-launched cone-cylinder test vehicle and 6-KS-3000, T-40 type rocket engine.

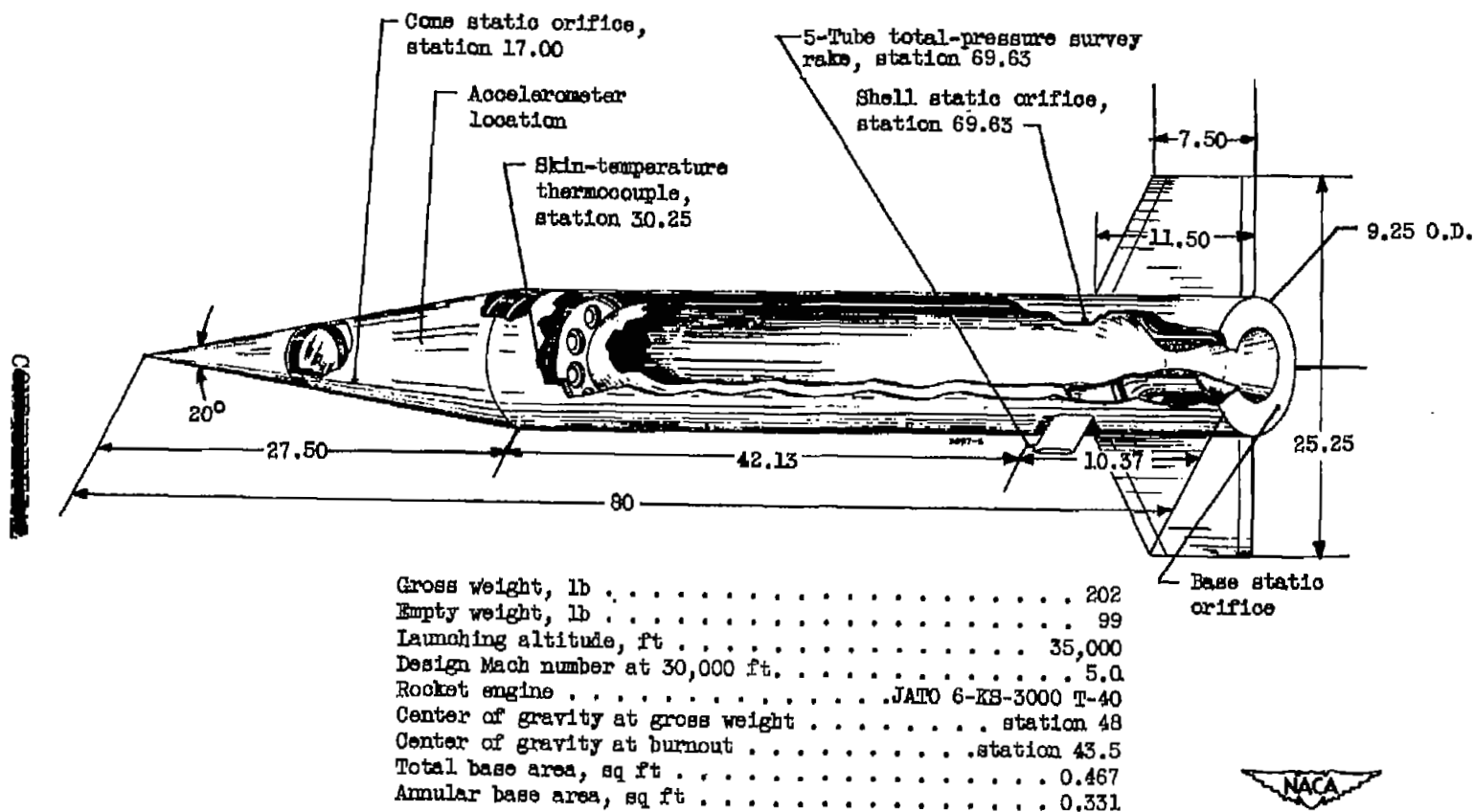


Figure 2. - Schematic sketch of air-launched cone-cylinder test vehicle including general specifications and location of instrumentation pickups. (Dimensions are in inches.)

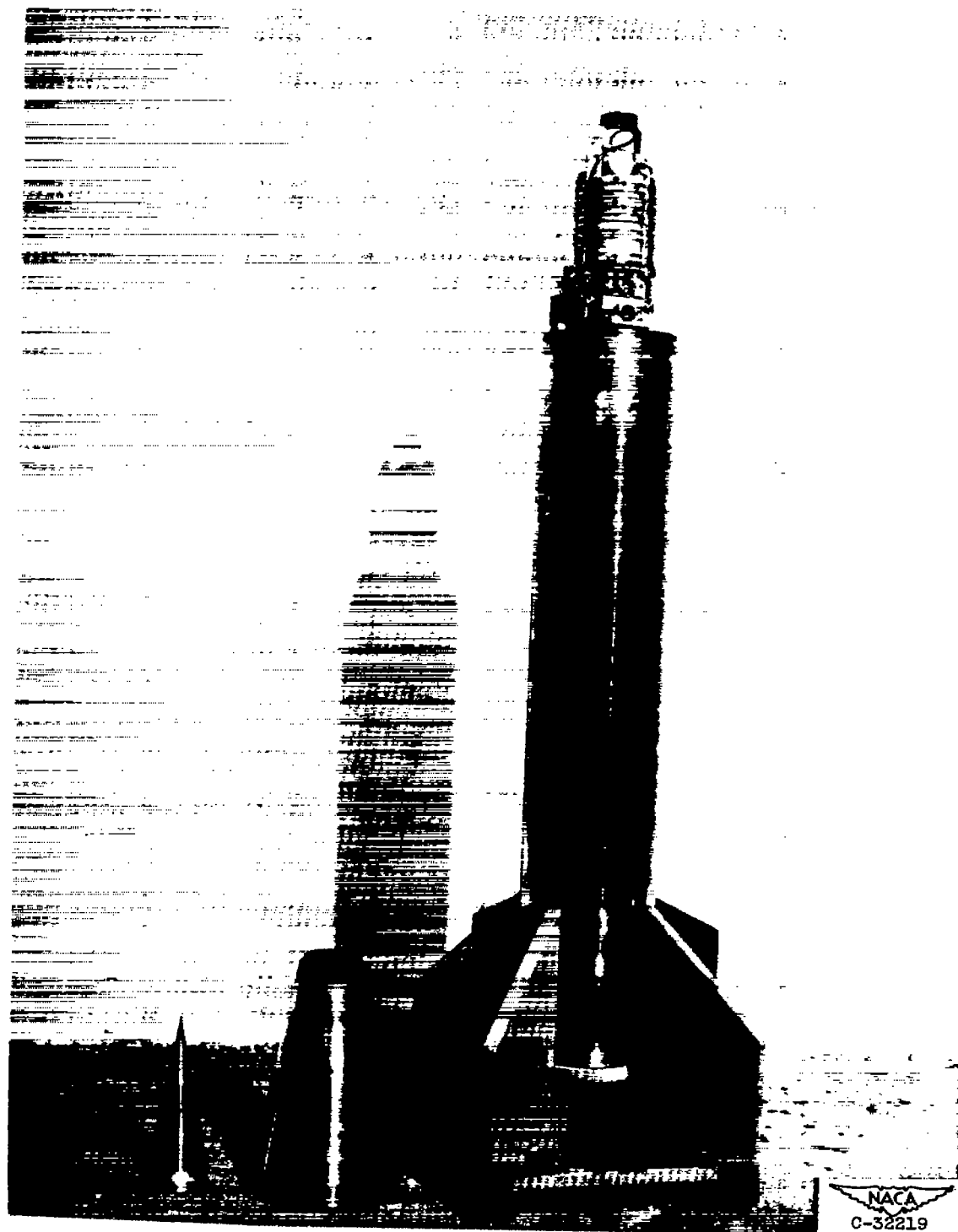
~~CONFIDENTIAL~~

Figure 3. - Disassembled view of air-launched cone-cylinder test vehicle illustrating location of telemetering unit.

~~CONFIDENTIAL~~

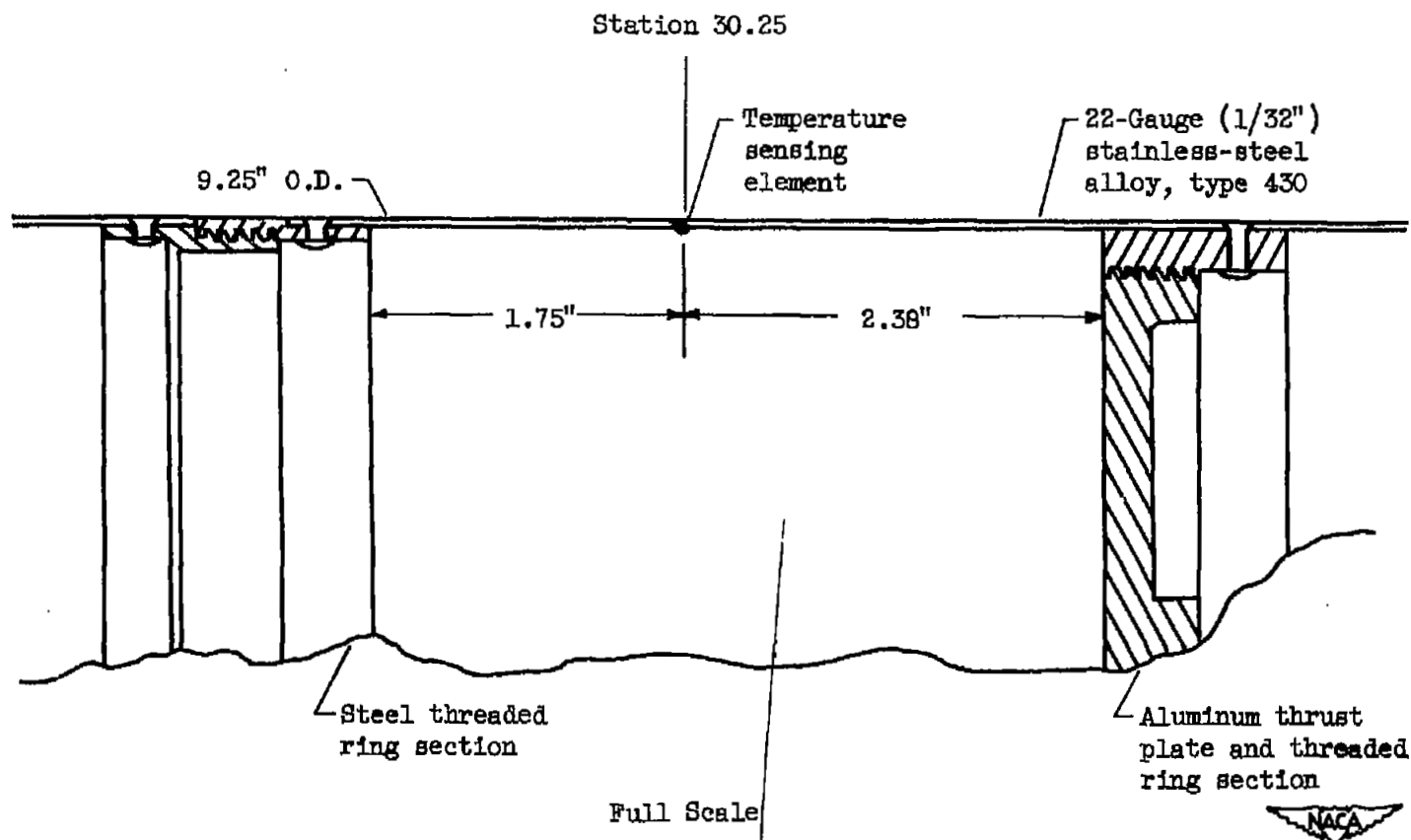


Figure 4. - Sketch of skin-temperature pickup location of air-launched cone-cylinder test vehicle.



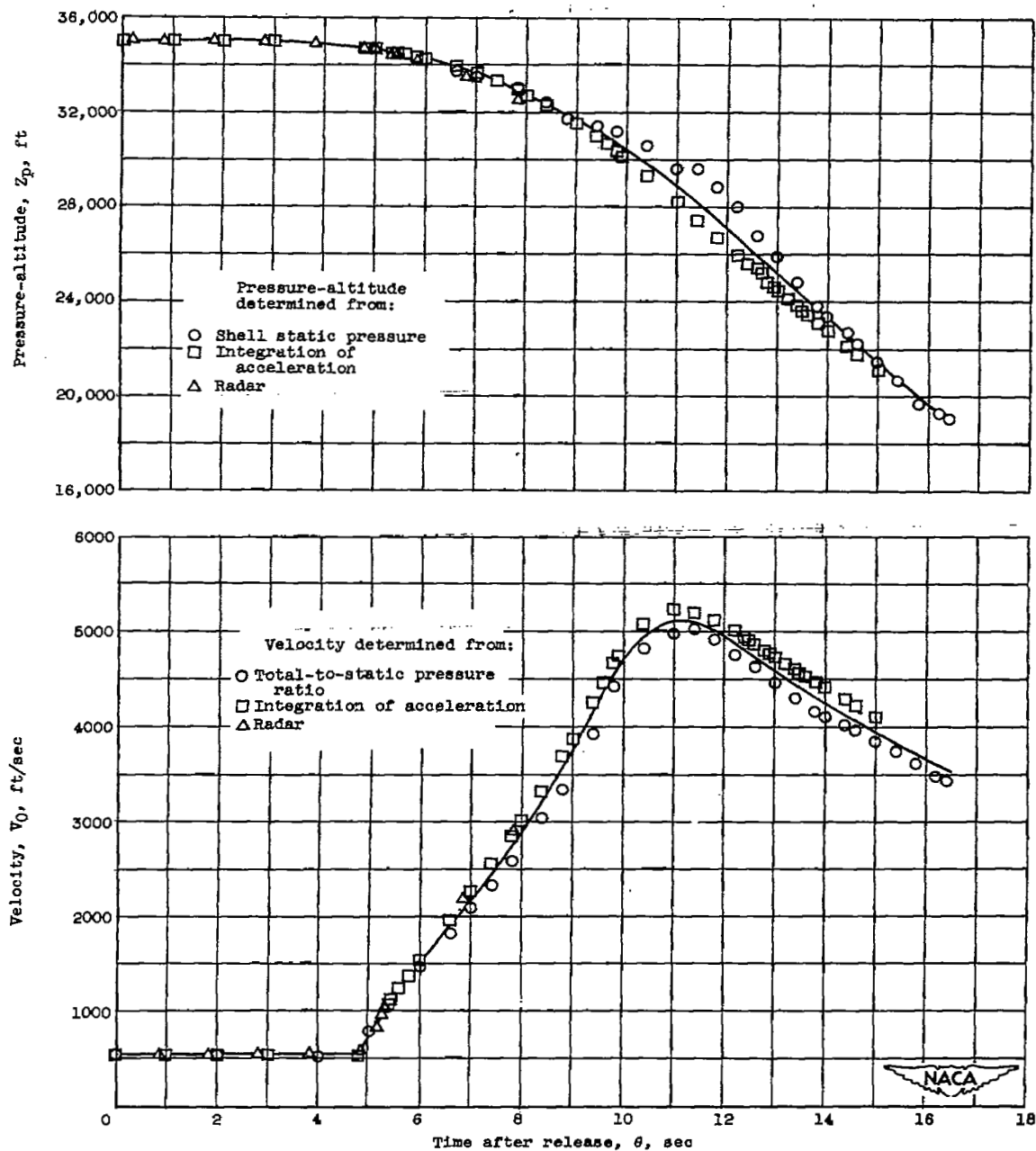


Figure 5. - Time history of pressure-altitude and velocity of air-launched cone-cylinder test vehicle.

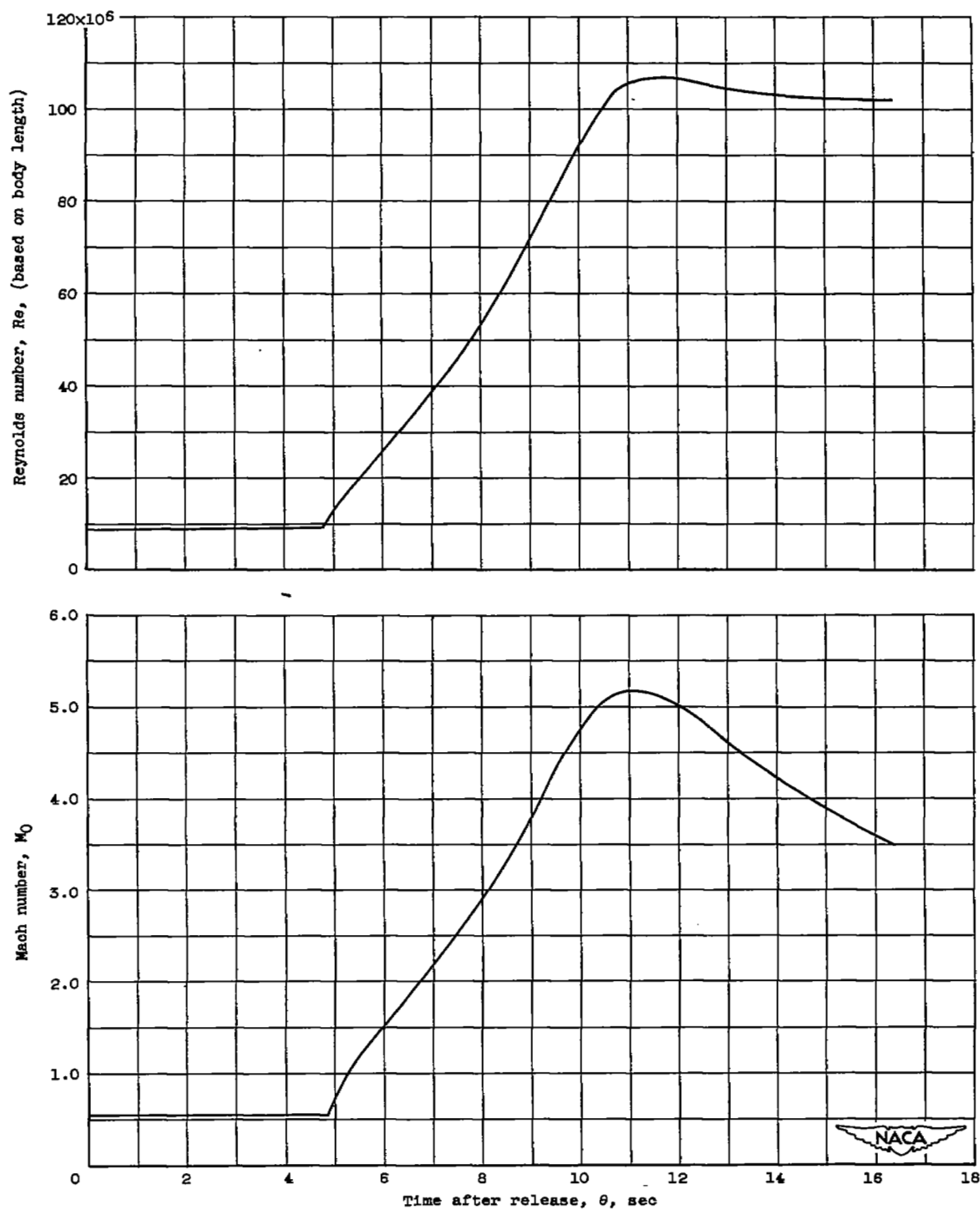


Figure 6. - Time history of free-stream Mach number and Reynolds number of air-launched cone-cylinder test vehicle.

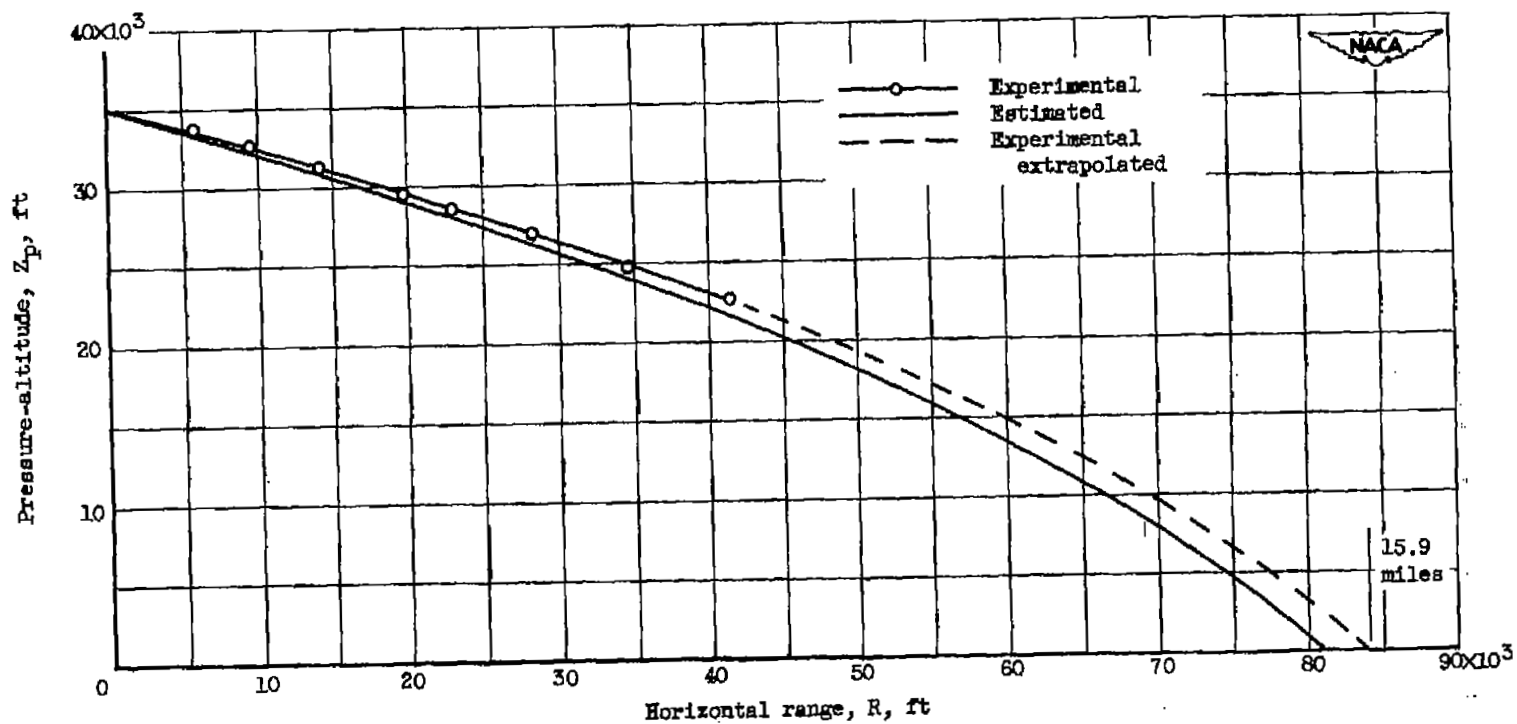


Figure 7. - Trajectory of air-launched cone-cylinder test vehicle as compared with estimated trajectory.

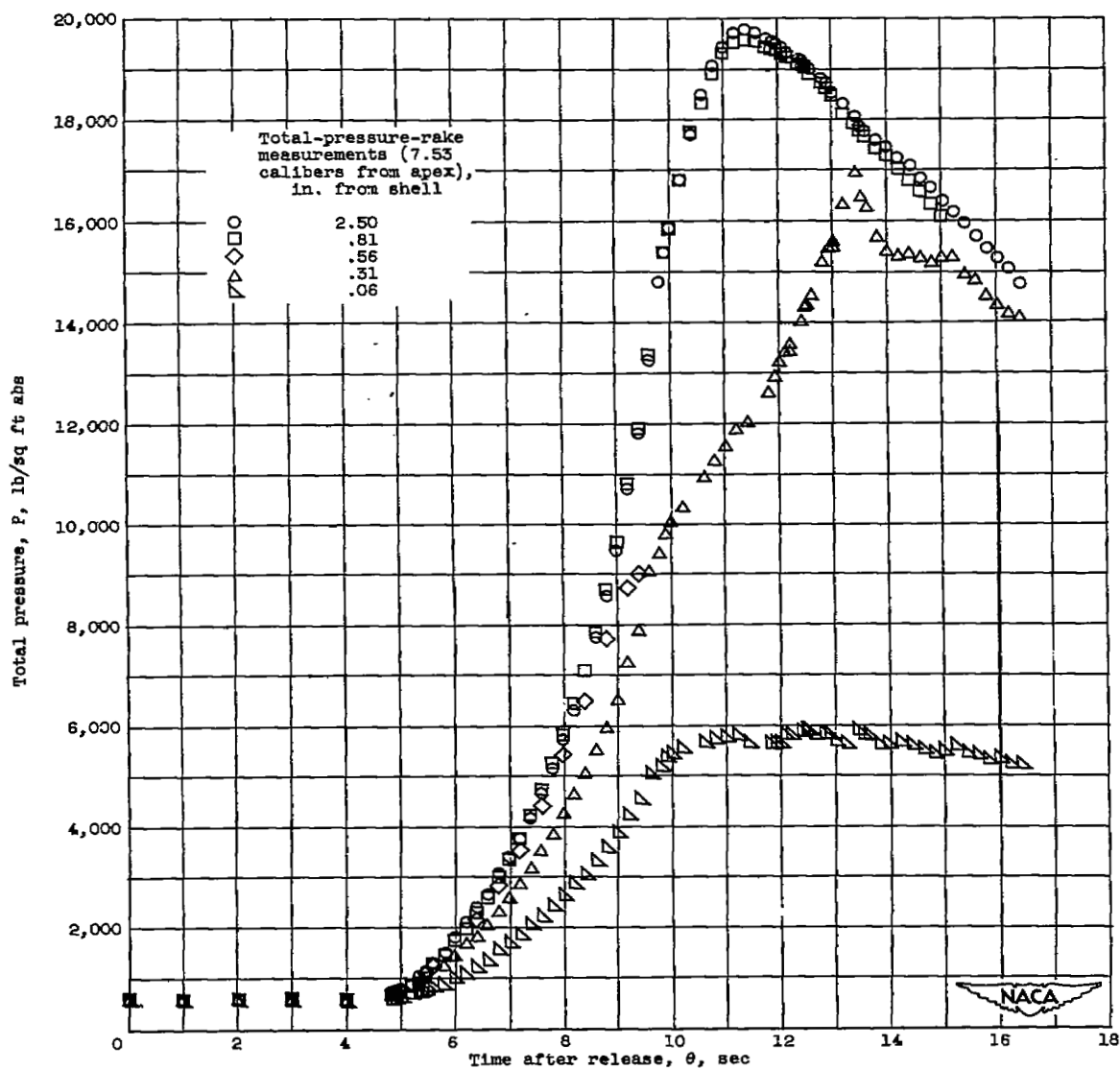


Figure 8. - Time history of total pressures measured during flight of air-launched cone-cylinder test vehicle. (Data have not been corrected for shock losses.)

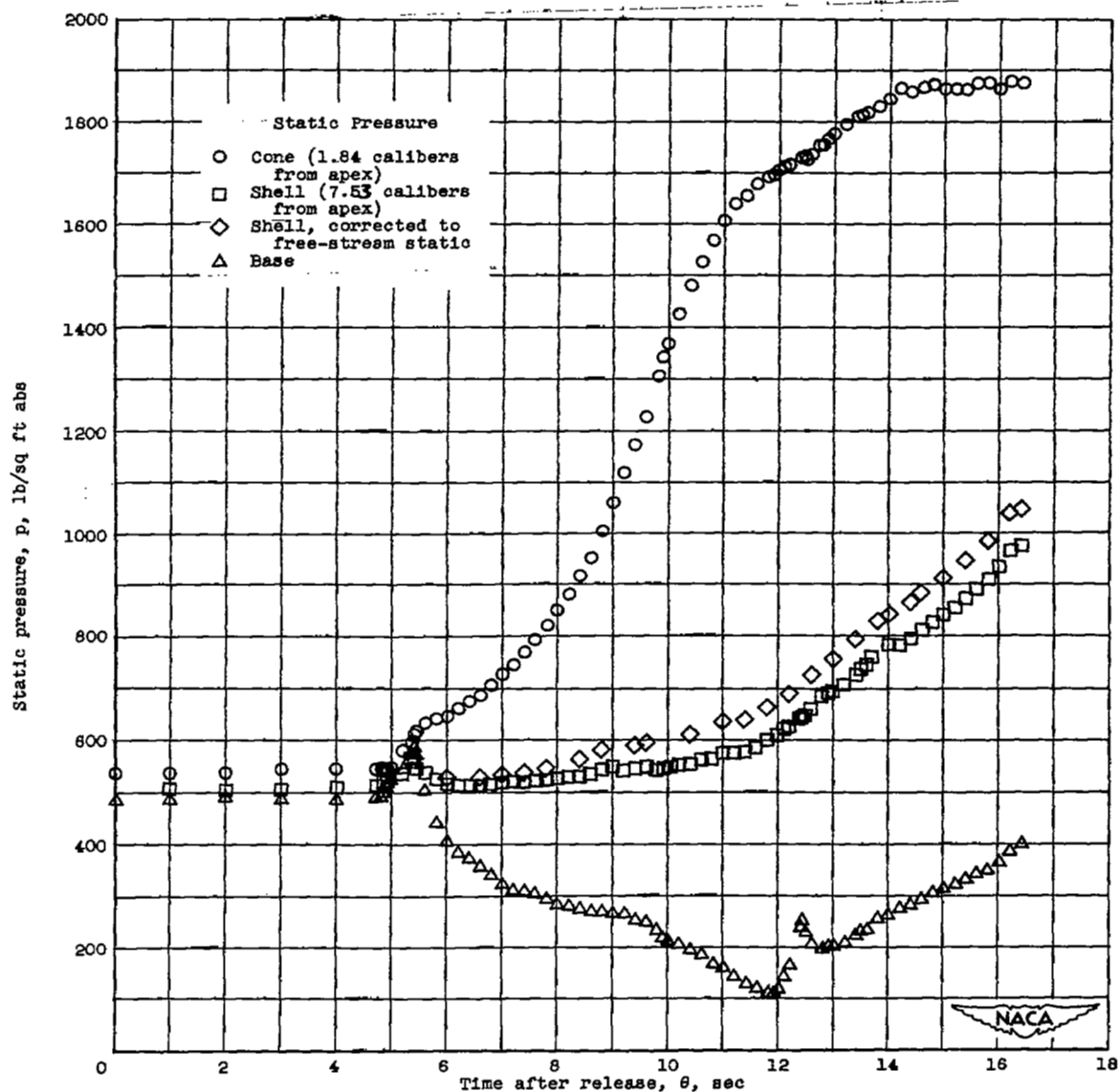


Figure 9. - Time history of static pressure measured during flight of an air-launched cone-cylinder test vehicle.

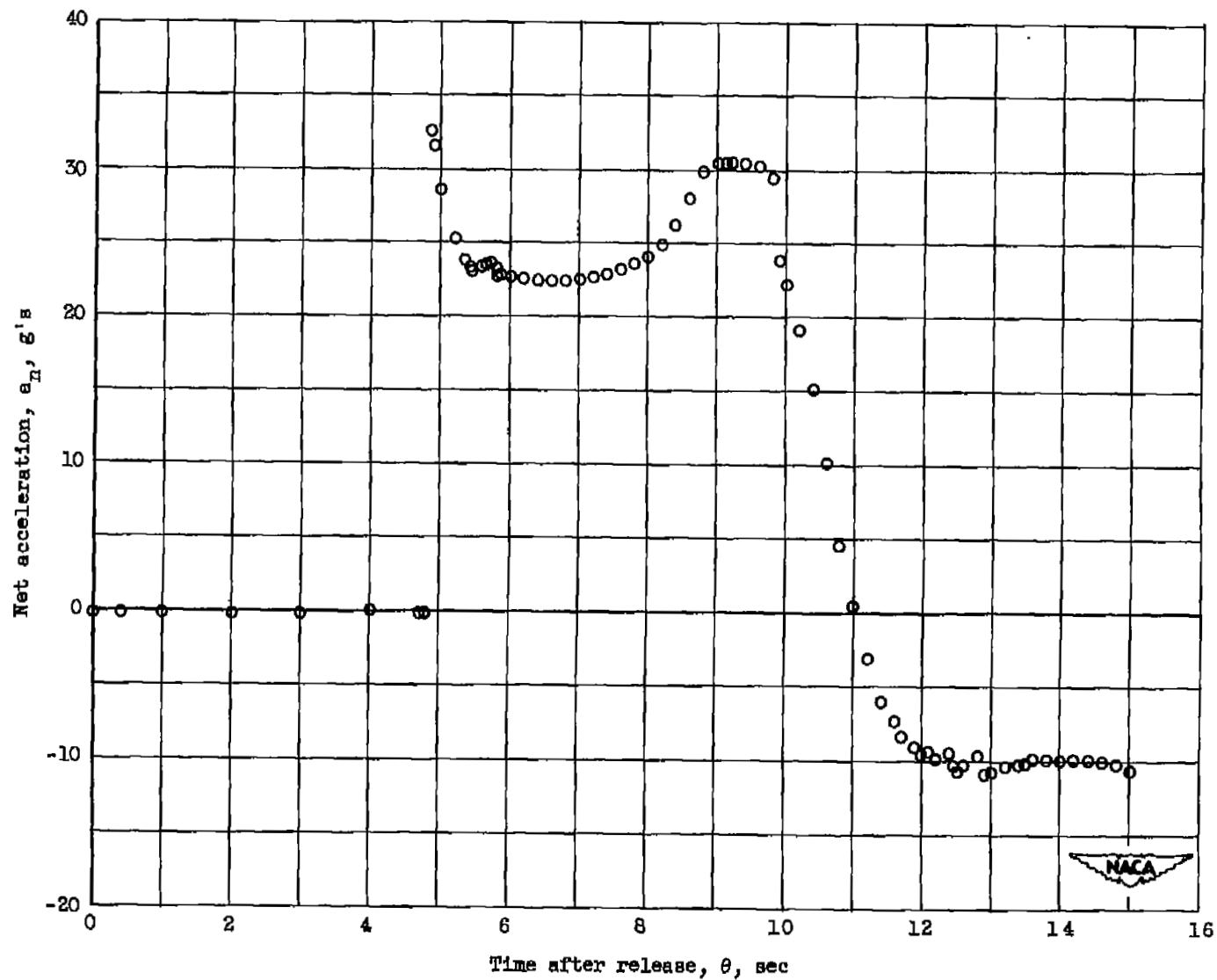


Figure 10. - Time history of net acceleration measured during flight of air-launched cone-cylinder test vehicle.

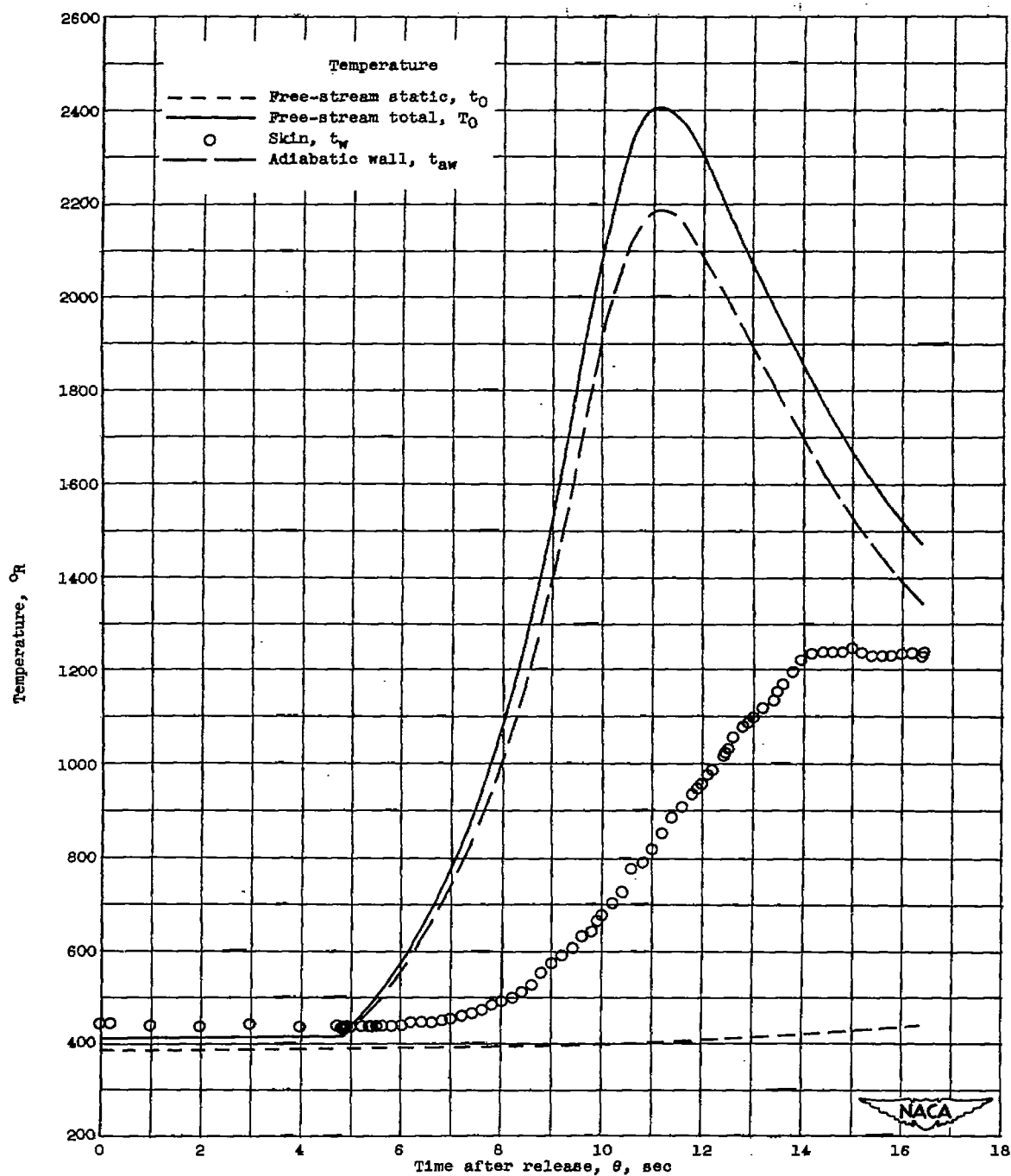


Figure 11. - Time history of air and skin temperatures encountered during flight of air-launched cone-cylinder test vehicle.

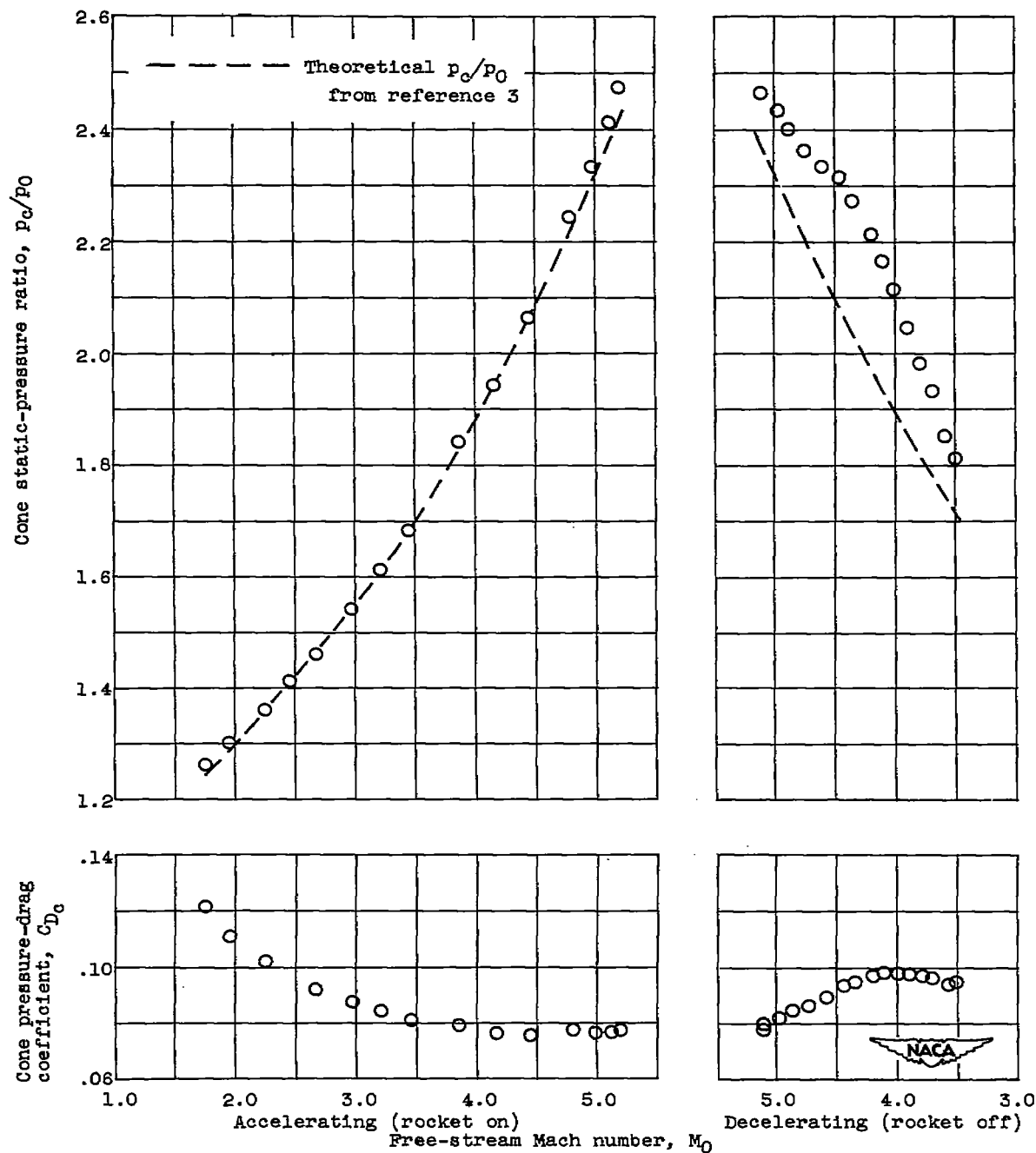


Figure 12. - Cone static-pressure ratio and cone pressure-drag coefficient as function of free-stream Mach number.



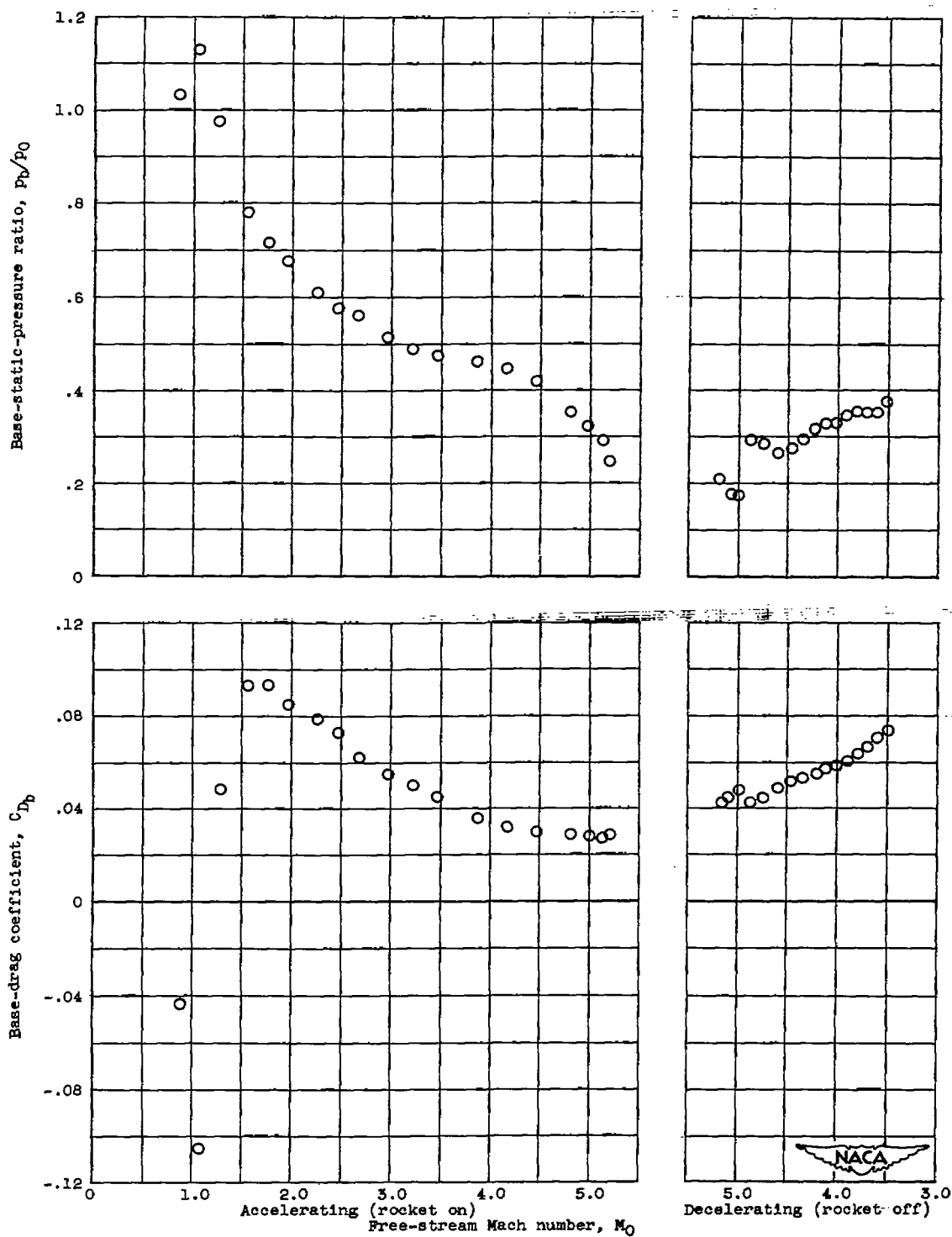


Figure 13. - Base-static-pressure ratio and base-drag coefficient as function of free-stream Mach number.

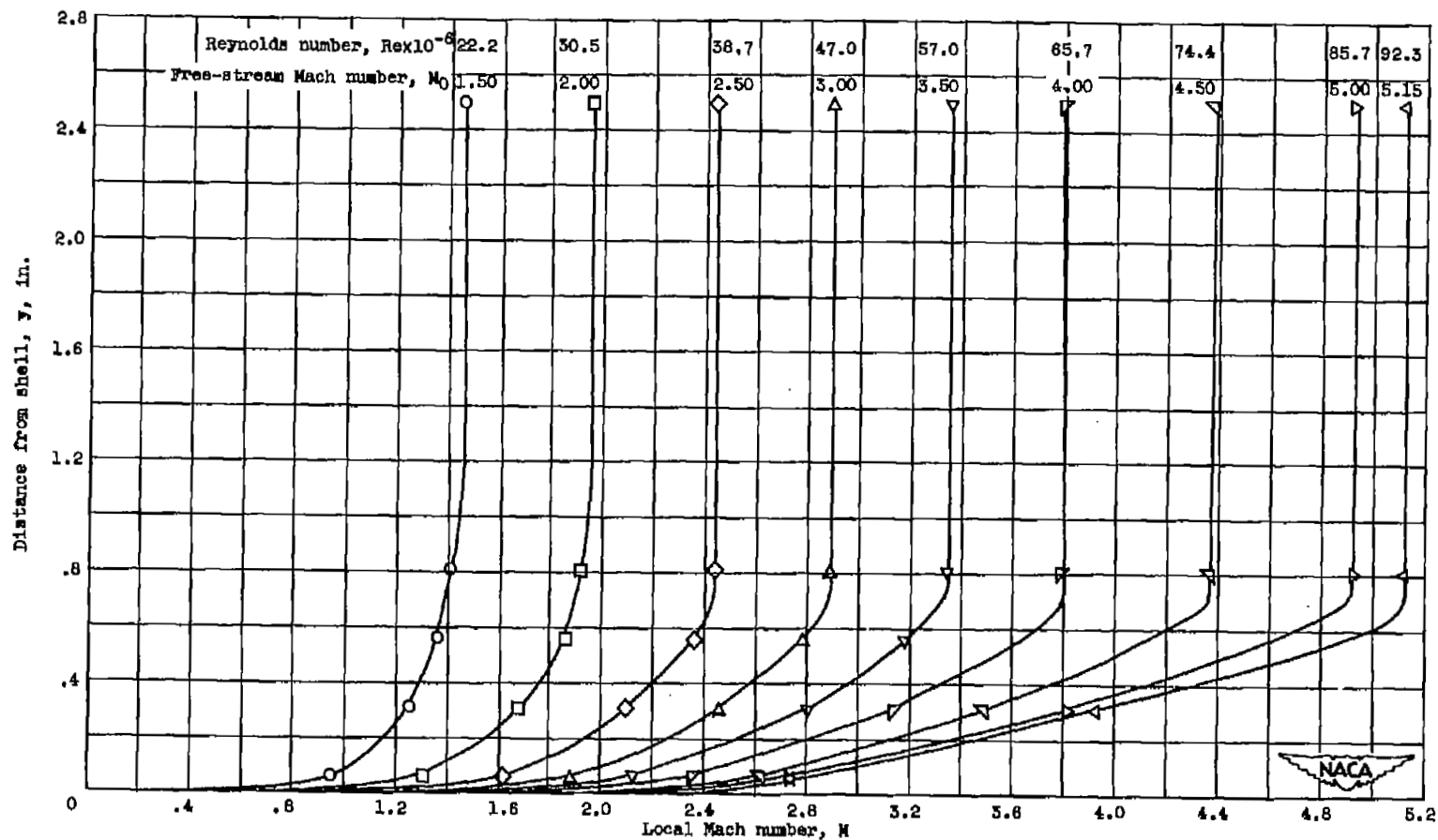


Figure 14. - Variation in local Mach number through boundary layer for free-stream Mach number range of 1.50 to 5.15. Reynolds number is based on body length to rake, station 69.83.

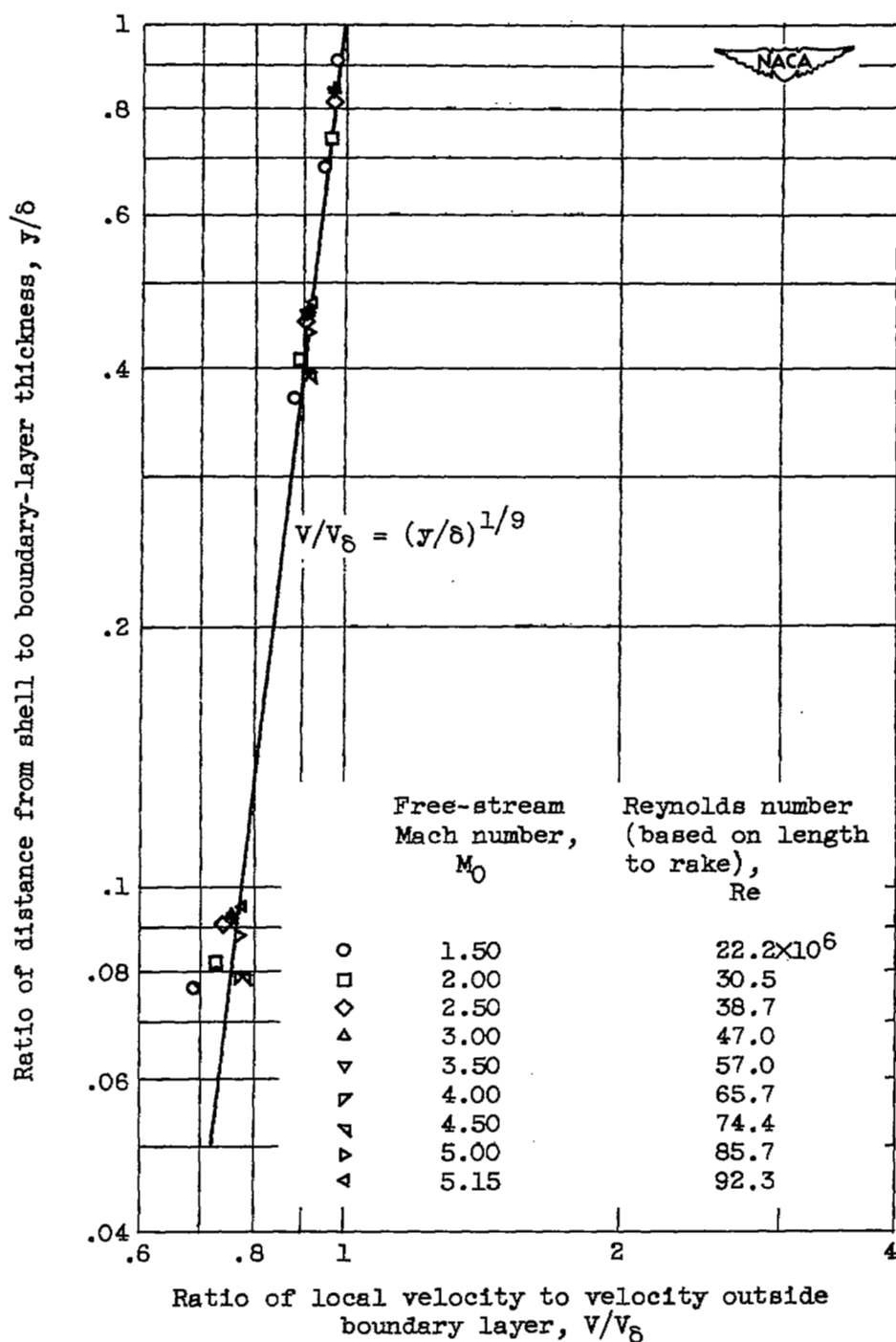


Figure 15. - Boundary-layer velocity profile for free-stream Mach number range of 1.5 to 5.15.

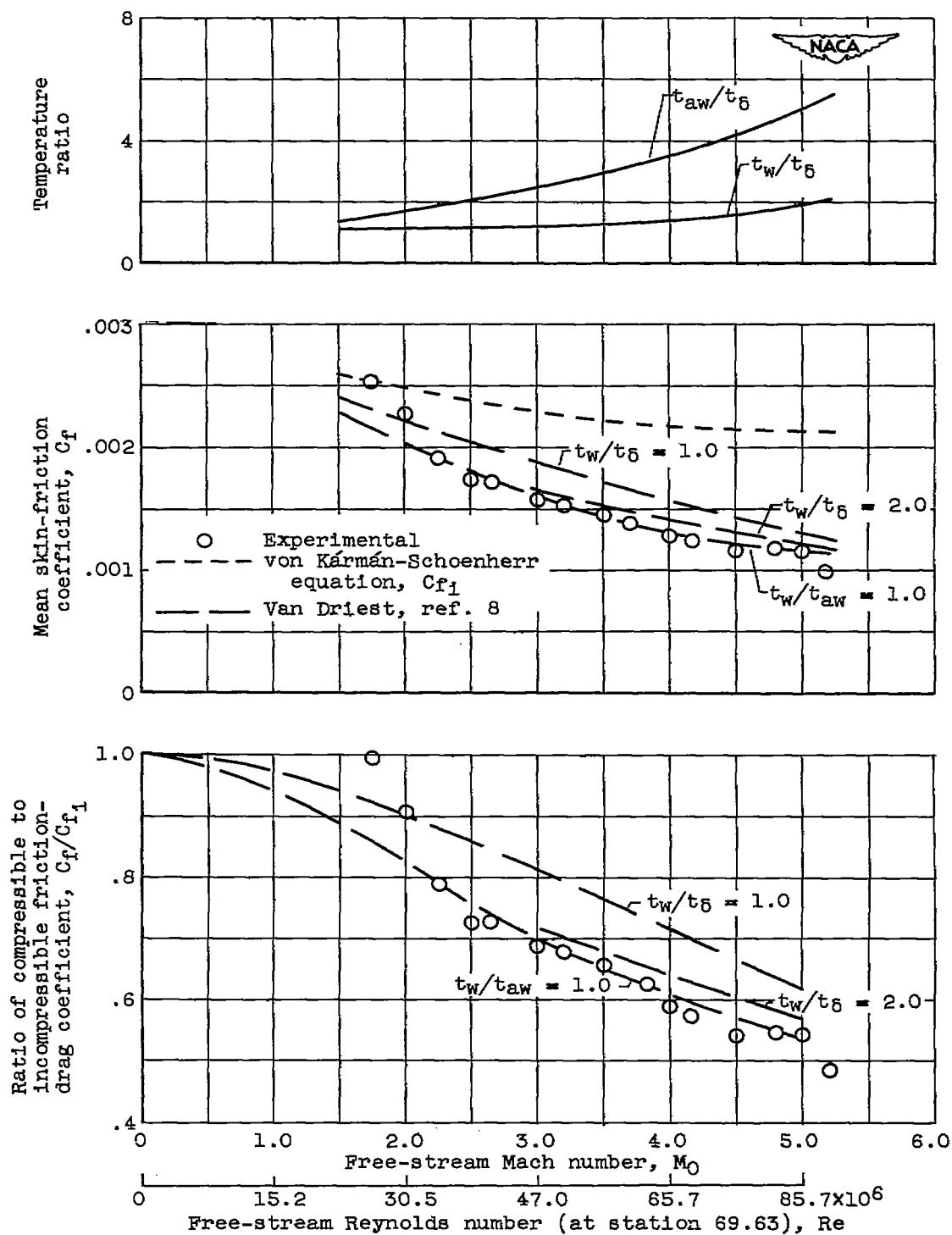


Figure 16. - Mean friction-drag coefficient as function of free-stream Mach number and Reynolds number.

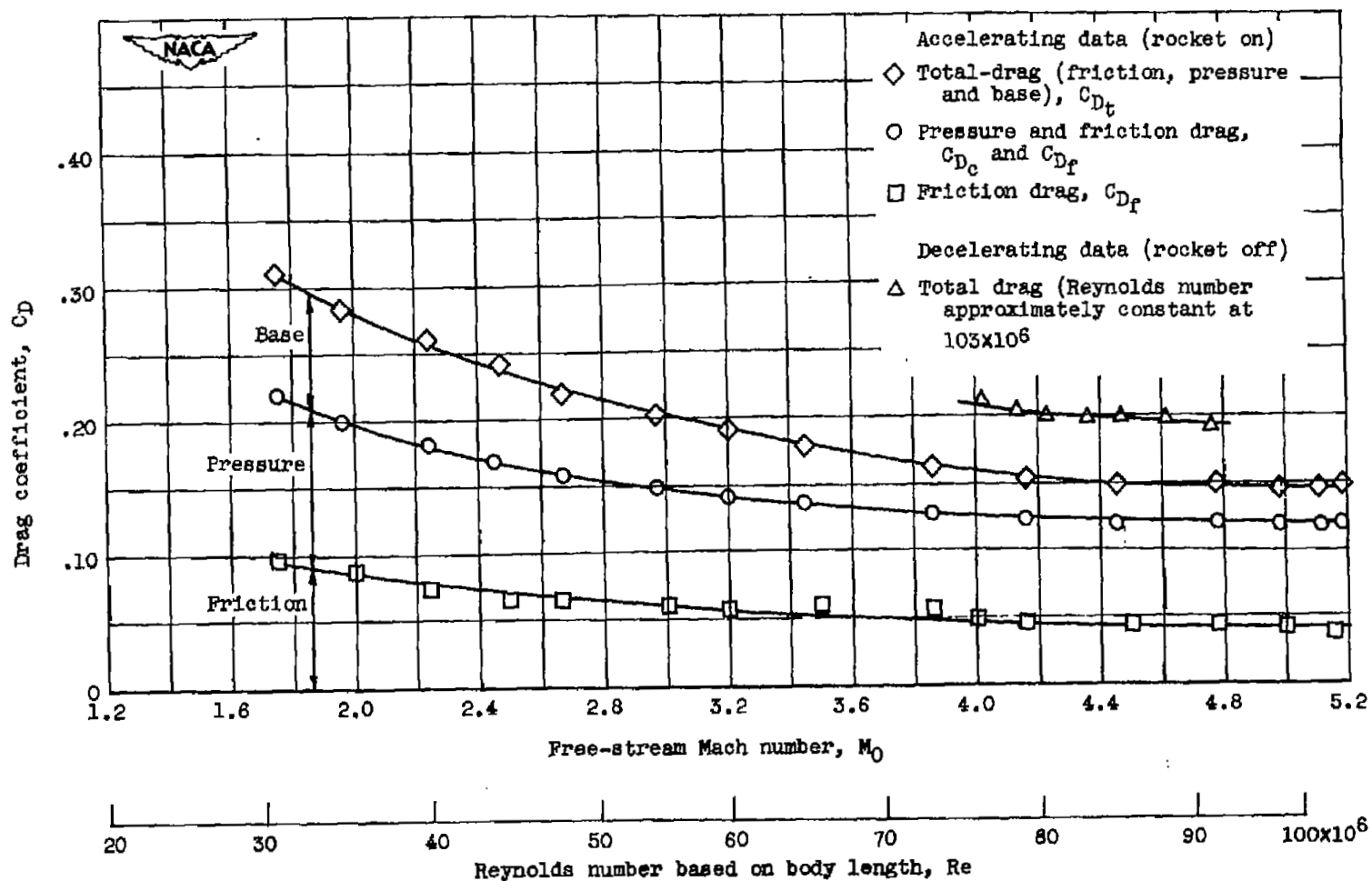


Figure 17. - Total and component drag coefficients as function of free-stream Mach number and Reynolds number.

3015

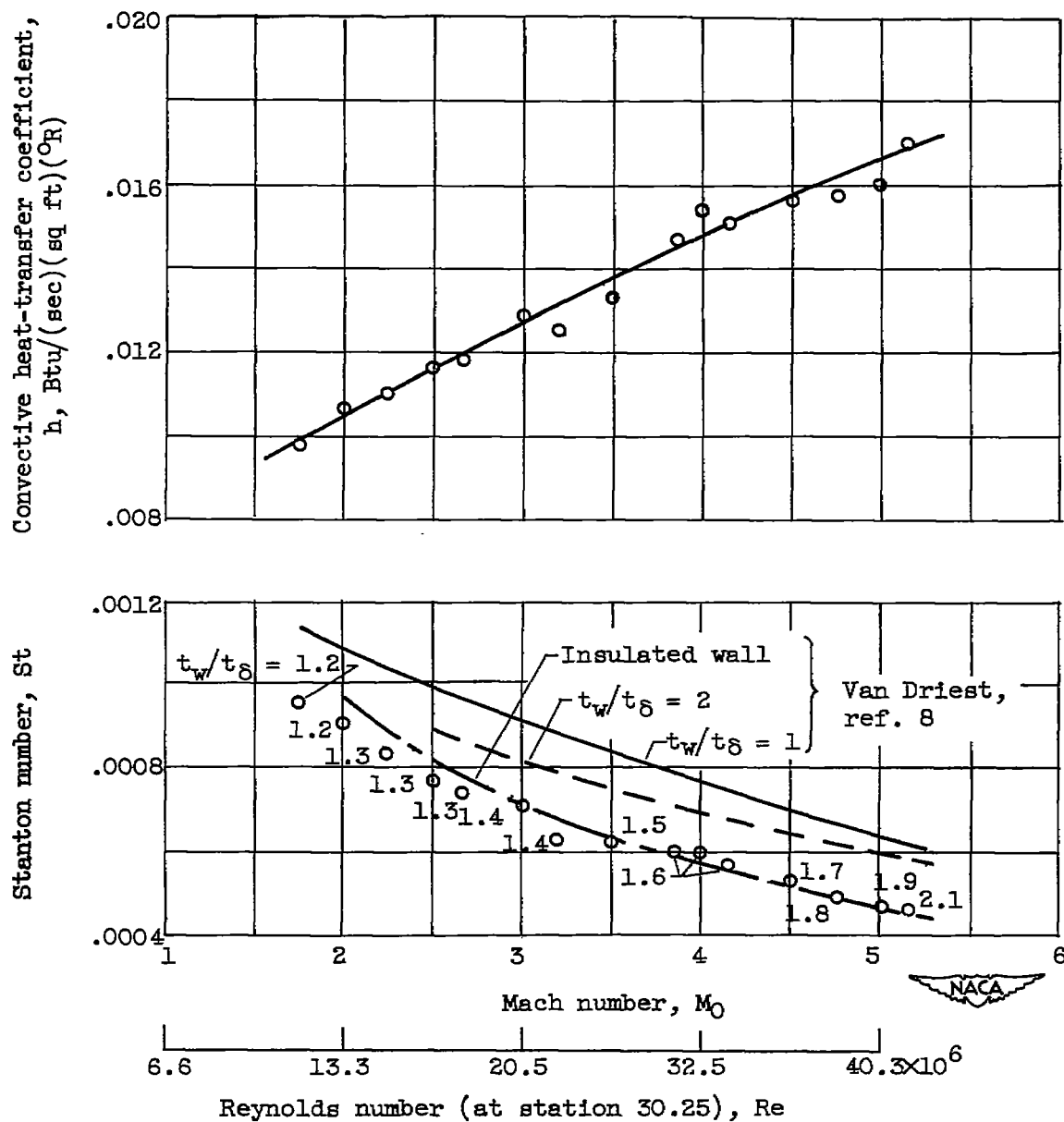


Figure 18. - Local convective heat-transfer coefficient and Stanton number as function of free-stream Mach number and Reynolds number.